Nucleation, pinning, and flow of vortices in Josephson-junction arrays with defects

Sujay Datta, Shantilal Das, and Deshdeep Sahdev
Department of Physics, Indian Institute of Technology, Kanpur 208 016, India

Ravi Mehrotra
National Physical Laboratory, Dr. K. S. Krishnan Rd., New Delhi 110 012, India

(Received 24 April 1996)

We numerically study the properties of two-dimensional overdamped Josephson-junction arrays *containing* defects. We employ fast algorithms adapted to arrays with defects. In arrays as large as 128×256, we investigate the vortex pinning regime, the transition from the superconducting to the resistive state and various finite size effects. Owing to the highly anisotropic nature of the pinning potential in rectangular arrays, we observe pinned vortices in arrays much smaller than expected so far. The energy of the array changes discontinuously at transitions across vortex sectors that are characterized by the number of pinned vortices. These pinned vortices also cause hysteresis in the array which we investigate in some detail. The periodic regime reveals the nature of waves which carry the vortices. Finally, an analysis of extended and distributed defect patterns affirms the analogy of current driven arrays with hydrodynamic flows. [S0163-1829(96)01942-X]

I. INTRODUCTION

The properties of Josephson-junction arrays (JJA's) have recently come under close scrutiny from various research groups,[1] owing partly to the fact that large arrays can now be fabricated with controlled variation of junction parameters in various sizes and shapes.[2] The large body of high precision experimental data, which has, consequently, become available has in turn stimulated much theoretical and numerical research. This has dealt both with the statics[3] and dynamics[4–8] of these arrays. While Monte Carlo studies[4,5] of such systems have looked, for example, at the vortex lattice produced by an external magnetic field, the study of effects away from equilibrium has focused, among other things, on the dynamical properties of JJA's in the presence of controlled[6] and random disorder.[7,8]

In accordance with Forrestor *et al.*[9] we note that disorder can be introduced into JJA's in three ways: (i) bond disorder in which the coupling strength of individual junctions is varied, (ii) positional disorder in which the vector potential entering via an external magnetic field takes on random values, and (iii) bond dilution in which certain junctions are eliminated altogether. Bond disorder has been studied by Berge[10] to distinguish between the Ising and the Kosterlitz-Thouless (KT) transition temperatures in fully frustrated square lattices and by Chung *et al.*[11] and Li *et al.*[12] who find that disordered arrays have a higher resistance than perfect ones. Positional disorder has, similarly, been investigated in various contexts by a number of authors. Reentrant glassy behavior in the temperature versus disorder-parameter plot for positionally disordered arrays has been predicted by Granato *et al.*[13] and investigated experimentally by Benz *et al.*[14] It has further been found that such arrays lead to the formation of a novel vortex pattern far from equilibrium[7] as also to a plasticlike flow of vortices.[8] Experiments on the critical behavior of randomly bond-diluted arrays[15] have revealed that disorder of this type does not destroy the scale invariance of the KT transition. Finally, Leath *et al.*[16] have discovered that the transition to resistive behavior in arrays with missing junctions occurs only when the external current reaches a value for which a vortex path spanning the entire sample becomes possible. This is in contrast to breakdown phenomenon in fuse networks and other linear systems, wherein breakdown emanates from the most critical defect and spreads outwards.[17] They have also found that current flow past a row of missing bonds in an otherwise perfect array gives rise to voltages on becoming resistive. The behavior of voltages changes from periodic to quasiperiodic and eventually chaotic, as the vortex ''street,'' in the corridor containing the defect, spreads to adjacent columns.

In this paper, we investigate additional effects of bond disorder and dilution in current driven overdamped JJA's. Some of these results were briefly reported earlier.[18] More specifically, we study, through computer simulations, the behavior of vortices in the superconducting regime, i.e., their nucleation, movement, and pinning. We do this for arrays much larger than those studied previously. We find that the time-independent states of uniformly driven arrays with linear defects, created through bond disorder *or* dilution, fall naturally into various sectors, separated by kink discontinuities in energy. Each sector is characterized by a fixed number of pinned vortices. These pinned vortices produce a hysteresis in the system, which we explore in some detail. Several complementary insights into each of these phenomena are obtained by keeping track of the changes in phase variables caused by modifications in current drive. Studying these changes carefully in the (resistive) periodic regime, in addition to the superconductive one, accords us a deeper understanding of how the breakdown of superconductive flow actually occurs. We find, for instance, that the periodic flow of vortices is sustained by the absorption of energy present in spin waves. Finally, we examine current flow past extended defects. We find that in some cases *increased* bond dilution can *enhance* the magnitude of i_c, the critical current for the breakdown of superconductive flow in the array, provided the current flow around the extended defect is more stream-

lined. This effect has obvious analogues in hydrodynamic flows.

The paper is organized as follows. In Sec. II, we present the model employed and an outline of the fast algorithm used in the numerical studies. In Sec. III, the studies on linear defects with graded and broken bonds, transitions to various vortex sectors, and the periodic regime are discussed. In Sec. IV, current flow past defects of various shapes is studied to explore streamlining properties in analogy with hydrodynamics. A summary and conclusions are presented in Sec. V.

II. THE MODEL

The evolution equation for the phases of the superconductors in the Josephson links is governed by the RSJ model[19,20] which divides the total current flowing through a junction into two ''channels:'' superconductive and resistive. We work at zero temperature and magnetic field ($T=0$, $B=0$). We also assume that the perpendicular magnetic field penetration depth for such arrays is large thereby neglecting self-shielding currents (applicable in case of SNS arrays). The superconducting channel carries a current $i_0 \sin\Delta\theta$ where i_0 is the critical current of a single junction and $\Delta\theta$ is the phase difference between the two superconducting sites. The resistive channel carries a current proportional to the voltage developed by the Josephson relation. The total current conserving dynamics[21] for the case of overdamped junctions thus leads to the evolution equation

$$\sum_{\langle jk\rangle}\left[\frac{\hbar}{2eR}\frac{d\theta_{jk}}{dt}+i_0\sin\theta_{jk}\right]=I_j^{\rm ext}\ \ \forall j, \tag{1}$$

where R is the shunt resistance, $I_j^{\rm ext}$ is the external current applied to the jth node of the array, and $\langle jk\rangle$ are the nearest neighbors of j. Using a nondimensional time $\tau=t(2eI_cR)/\hbar$, one can alternatively write the above equation in matrix notation as

$$G_0^{-1}[\dot\theta]=[d], \tag{2}$$

where $[\dot\theta]$ and $[d]$ are the the voltage and the divergence (inclusive of external currents, if any) vectors, respectively. Using the gauge condition $\Sigma_j\dot\theta_j=0$ one can invert the relation to get

$$[\dot\theta]=\widetilde{G}[d]. \tag{3}$$

The integration procedure thus involves the multiplication of an $N\times N$ matrix $\widetilde{G}$ with an $N\times 1$ vector $[d]$ at each time step leading to an complexity $\mathcal{O}(N^2)$. A faster $\mathcal{O}(N\ln N)$ method of integrating the above equations was evolved by Eikmans and Himbergen[22] which was later improved by Dominguez *et al.*[7] The case of bond disorder can easily be incorporated into such a formalism as it affects only the divergence term in Eq. (2) since $i_0\sin\theta_{jk}\rightarrow g i_0\sin\theta_{jk}$. We call such bonds ''graded'' bonds. Bond dilution due to missing bonds in the array, however, introduces internal boundaries making the above method inapplicable. This can however be solved[23] by noting that the corresponding evolution equation equation for the phases [see Eq. (2)] for an array containing one missing bond between sites $k\equiv(x_0,y_0)$ and $k+1\equiv(x_0+1,y_0)$ can be written in matrix form as

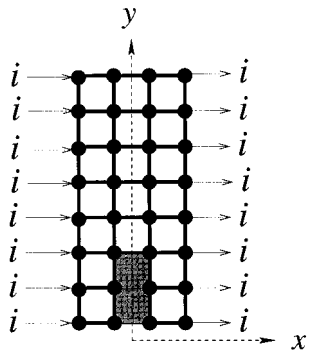

FIG. 1. Schematic of $y>0$ portion of a 4×16 array with an $n=4$ defect (shown by a shaded region). Full dots and thick lines joining them represent superconduting islands and Josephson junctions, respectively. Narrow lines inside the defect denote graded or broken bonds. Arrows marked i symbolize a current $i_{\rm ext}$ in the direction of the arrow.

$$(G_0^{-1}+h)[\dot\theta]=[d]. \tag{4}$$

Here the matrix G_0^{-1} is the discrete Laplacian for a *finite perfect* array with free boundary conditions [as in Eq. (2)] and h is given by $h_{k,k}=h_{k+1,k+1}=1$, $h_{k,k+1}=h_{k+1,k}=-1$ and $h_{i,j}=0$ otherwise. The form of h allows us to exactly solve for $[\dot\theta]$ in $\mathcal{O}(N\ \ln N+N)$ steps.[23] This procedure can further be extended to case of n missing bonds forming a linear defect.

We use the fast algorithms[23] to integrate the set of differential equations for arrays with defects of various kinds using a fourth-order Adams Moulton predictor-corrector method. Each integration time step is 0.05–0.1τ and a typical run is carried over 100 000 time steps. In addition, we use sparse matrix routines[24] to store G_0 and other large matrices for the case of bond dilution. This reduces the computer memory storage requirements significantly.

It is worth noting that the case of bond dilution and disorder introduces various time scales into the problem. Since, τ is a function of i_0, the time scale of each defective junction is different. On the other hand, positional disorder introduced by a transformation of the gauge variables, $\theta_{ij}\rightarrow(\theta_{ij}-A_{ij})$, introduces various length scales caused by the presence of such disorder at different bonds.

III. LINEAR DEFECTS

Using the fast algorithms, we have numerically studied[25] large $N_x\times N_y$ arrays (as big as 128×256 in size) with linear defects of varying sizes. A typical geometry is shown in Fig. 1. A linear defect, consisting of n graded-broken bonds all parallel to the x axis, is placed symmetrically along the central column (CC). The current drive $i_{\rm ext}$ is uniform along the left edge. We have taken advantage of the symmetry, $\theta(x,y)=\theta(x,-y)$, about the x axis to speed up the simulations.[26] We thus calculate only the $y>0$ section of the array. A positive vortex located at (x,y) has a negative image vortex located at $(x,-y)$ due to this symmetry. While this symmetry exists for all the configurations we study in this paper (verified through numerical simulations on full size arrays), it is important to realize that it *does* break under

certain circumstances. For example, a periodic attractor corresponding to a collective vortex state with broken reflection symmetry has been identified for JJA's with defects, in the presence of a combined ac and dc current drive.[7,27,28] We have further found that the symmetry likewise breaks [along with the symmetry, $\theta(-x,y)=-\theta(x,y)$], once the array enters the chaotic regime. We do not investigate the latter in this paper. In fact, we explicitly monitor both $\theta(x,y)$ and $\theta(-x,y)$ to ensure that the array is not driven chaotic.

To be consistent with existing literature, henceforth, all array and defect sizes refer to the size of the full array and the defect even though the calculations are done only on half the array. The number of vortices and their description, however, pertains only to $y>0$ section of the array. All currents are scaled in units of i_0.

A. Graded defects

Here we explicitly show that vortices can be pinned inside a linear defect of graded bonds. This pinning in turn increases the magnitude of i_c for the system signifying a greater stability. We first study the steady-state regime of an array with a linear defect of uniformly graded bonds with grading g.

While this form of grading can be studied computationally with ease, it should be pointed out that verifying our results experimentally will require special arrays. Indeed, the Ambegaokar-Baratoff relation[29] tells us that I_cR is a constant determined by the superconducting gap, $\Delta(0)$ at $T=0$, and each time we vary I_c for a material with a given $\Delta(0)$, the shunt resistance R changes proportionately. Thus, to keep R fixed, we must vary $\Delta(0)$, i.e., create the defect out of a material different from the bulk. This could be done by depositing the relevant materials successively, in the presence of masks which are complements of each other. This procedure will, however, give rise to a series of heterogeneous junctions all along the edge of the defect. Such junctions are characterized at low temperatures predominantly by the material with the smaller value of $\Delta(0)$. This in turn means that, while this method can yield graded linear defects with a higher value of I_c than the bulk, it inevitably grades, for the case of a lower I_c, all the bonds on the defect's boundary as well. In view of this, we have additionally studied the more realistic defect geometry. We find that the qualitative features of the dynamics—vortex nucleation and pinning inside the defect—remain unaltered but the detailed description becomes more involved. For simplicity of presentation, we discuss only the case of a strictly linear defect.

We should also mention that with slight modifications in existing algorithms it should be possible to study defects in which I_c and R are both varied in keeping with the Ambegaokar–Baratoff relation. A detailed study of this kind will be presented elsewhere.

The variation of i_c, the critical current for the breakdown of superconductive flow in the array, with g is shown in Fig. 2 for a 64×64 array with 20 graded bonds forming a linear defect. The most striking feature of the curve is minimum at $g=g_m$. Intuitively, one would have expected i_c to decrease monotonically with g since a smaller value of g implies a reduced capacity to carry a supercurrent. However, this is clearly not the case. To understand the origin of this minimum, it is useful to examine the behavior of the phases θ at a number of relevant sites.

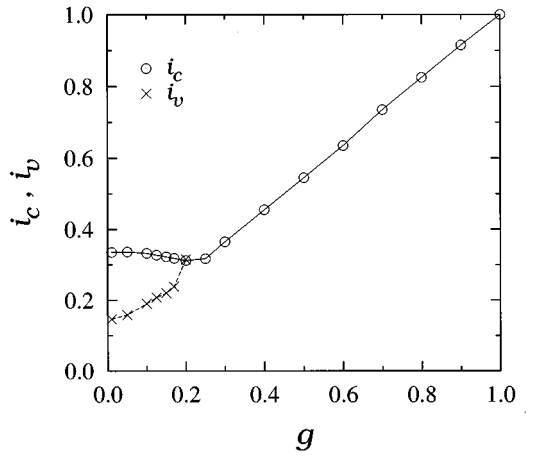

FIG. 2. A plot of i_c and i_v vs g showing the minimum in i_c for 64×64 array with a linear defect consisting of 20 graded bonds. The lines through the symbols are a guide to the eye.

For very small values of $i_{\rm ext}$, the x-bond current in the CC decreases monotonically from a maximum at the center of the defect to $\sim i_{\rm ext}$ at large values of y. In other words, the θ's along the left edge of the central corridor (LECC) are arranged [see Fig. 3(a)] in a monotonically decreasing sequence (while those along the right edge are just their negatives[26] and the phase differences across x bonds are twice the LECC phase values). As $i_{\rm ext}$ increases, so does each of these phase angles. Eventually, for $i_{\rm ext}=i_1$, the phase, θ_1 at the site $(-1/2,1/2)$ (see Fig. 1) reaches a value of $\pi/4$ and the current $\sin(2\theta_1)$ in the corresponding x bond becomes unity, i.e., it turns critical. As $i_{\rm ext}$ is raised beyond i_1, the phases simply go on increasing. As a consequence, $2\theta_1$ goes into the second quadrant and the current in the junction begins to fall. Thus, the criticality of a single junction does *not* mark the onset of dissipation, as also noted by Leath and Xia.[16] However, in contrast to their observations, this criticality is *not* accompanied by the formation of a vortex. A further increase in $i_{\rm ext}$ causes the next few bonds in the corridor away from the center to successively carry the critical current. This phenomenon persists until $i_{\rm ext}$ reaches a value i_v, θ_1 becomes equal to $\pi/2$ and the current in the junction drops to zero. As soon as $i_{\rm ext}$ exceeds i_v, the current becomes negative and a vortex appears since the next x bond still carries a positive current and there is a current circulation in the central plaquette located at (0,1). The behavior of this vortex now depends on whether $g>g_m$ or $g<g_m$. For $0<g<g_m$, the vortex remains pinned inside the defect [Fig. 3(b)] with the pinning center shifting to larger values of y as g increases. Eventually, at $g=g_m$, the pinning occurs just outside the defect at its tip. For $g>g_m$, there is no pinning at all. We notice, however, that the vortex is never pinned at its point of nucleation even as $g\to0$.

Finally, for $g<g_m$ but $i_v<i_{\rm ext}<i_c$, the pinned vortex moves outwards, only to get pinned again, always inside, or at most at the edge of the defect. At $i_{\rm ext}=i_c$, the Lorentz force on a vortex at any point along the CC exceeds the

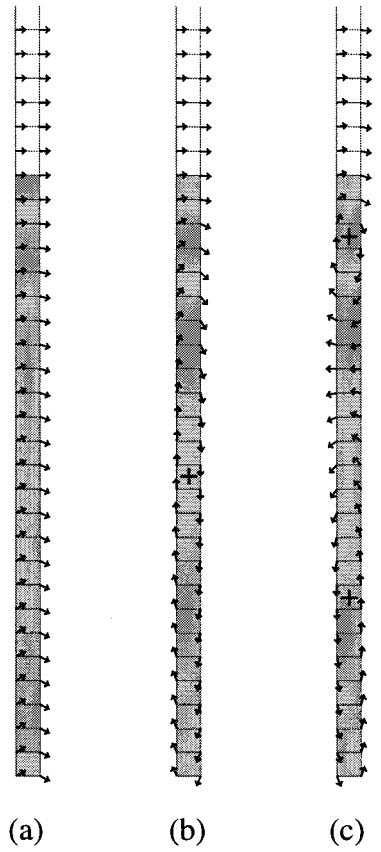

FIG. 3. Typical configuration of phases in the central corridor of a 32×128 array with a $n=50, g=0.1$ graded defect. Only a portion of the corridor is shown for clarity. The shaded region corresponds to the defect. The vortices are marked with a + sign: (a) $i_{\rm ext}<i_v$, (b) $i_v<i_{\rm ext}<i_c$. The number of pinned vortices in (a), (b), and (c) are 0, 1, and 2, respectively.

pinning force. Consequently, the vortex moves all the way out to the edge of the array and begins to cause dissipation.

The i_v vs g curve (see Fig. 2), on the other hand, does not show any minimum. For $g>g_m$ the i_v and the i_c curves are coincident but separate out for $g<g_m$. We thus infer that grading causes the pinning of vortices which in turn raises the i_c of such systems. This is quite in conformity with the case of continuum superconductors where vortex pinning centers are artificially created (e.g., by ion bombardment[30]) to avoid dissipation. What is surprising, however, is that $g_m\sim0.2$ is independent of the lattice and defect size provided the latter is small compared to N_y. In the case of $n\sim N_y$ the vortices do not get pinned for *any* value of g due to the presence of edge effects in the array. Consequently, i_c for such an array increases monotonically with g without showing any minimum.

The profile of currents in the x bonds in the CC, for the case described above, suggest that it is possible to pin several vortices inside the defect for $g<g_m$ provided the latter is sufficiently long. In accordance with this expectation, we have found that for a long narrow array 16×128 with $n=60$, $g=0.05$, and $i_{\rm ext}=0.0404$, we get as many as three vortices pinned inside the defect [as in Fig. 3(c) which shows the presence of 2 vortices]. After the formation and the movement of the first vortex, the magnitude of θ_1 at the center of the array once again passes through the same cycle of events to produce a second vortex which forces the first one outward. From a plot of the x-bond current in the CC versus y, one can easily locate the pinned vortices since these are clearly situated wherever a change in sign of the bond-current occurs.

B. Broken bonds

We next investigate the behavior of arrays in the presence of a linear defect produced by bond removal. It had been conjectured[16] that for infinite lattices, the pinning of vortices nucleated by a defect of this type, would occur for defect sizes ~200. With the fast algorithm outlined in Sec. II, we are in a position to check this out.

To begin with, we observe that the sequence of events described in Sec. III A is followed for this system as well, with some minor differences: The vortices are now formed at the tip, rather than the center, of the defect and their subsequent behavior depends on the value of i_v as compared to i_p, the depinning current required to overcome the potential barrier[31] for vortex motion from one plaquette to another. If $i_v<i_p$, the vortices are pinned by the lattice away from the defect. The transition to the periodic (resistive) state takes place at $i_{\rm ext}=i_c>i_v$. For $i_v>i_p$, the vortices move right across the central corridor, out of the array, and the transition to the periodic state takes place without any vortex pinning. In this case, i_c coincides with i_v.

We next describe how i_p, i_v, and i_c vary with N_x, N_y, and n. This dependence leads to an understanding not only of the $N_x, N_y\to\infty$ limit, but also of a number of finite size effects which are interesting in their own right.

We recall that Lobb *et al.*[31] calculated the potential barrier, E_B for a vortex to move from the center of one plaquette to the adjacent one for *square* arrays assuming a sinusoidal form for the pinning potential. The formalism of Rzchowski *et al.*[32] can be used to calculate $i_p=E_B/(2E_J)$ for various values of N_x, N_y, where E_J is the Josephson coupling energy. In carrying this out for vortex motion in the y direction, we find that for fixed $N_y=32$ and $N_x=4,8,16,32$, $i_p=0.147, 0.112, 0.102, 0.099$, respectively. Similarly for $N_x=32$ and $N_y=8,16$, $i_p=0.072, 0.093$, respectively. We thus see that in rectangular arrays, the finite size effects in the x and y directions are different, resulting in a highly anisotropic i_p, which can, for $N_x<N_y$, be larger than the infinite array limit of $i_p^\infty\simeq0.1$.[32] This implies that in finite arrays, it should be possible to observe vortex pinning for a defect of size smaller than $\simeq200$.[16] This is confirmed by our simulations, e.g., of a narrow 4×256 array with $n=22$. Here we observe as many as 10 pinned vortices lined up in the central corridor for $i_{\rm ext}=0.17\,396$, which incidently is much larger than i_p^∞

To isolate the effect of finite array size on i_c, it is expedient to define $\Delta i_c=i_c^\infty-i_c$, where i_c^∞ is the critical current in an infinite array. A log-log plot of $\Delta i_c/i_c^\infty$ versus N_x/n for a fixed $N_y/n=32$ is shown in Fig. 4. In obtaining this curve, we have taken $i_c^\infty=i_c(N_x=128)$ for all values of n considered. To convince ourselves that an array with $N_x=128$ is infinite for all practical purposes, we have checked that i_c varies by less than 0.3% and 0.002% as N_x is changed from

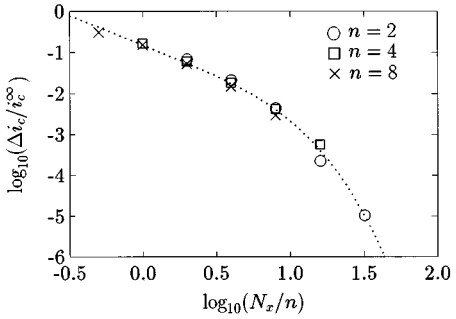

FIG. 4. A log-log plot of $(\Delta i_c/i_c^\infty)$ vs (N_x/n) for various n but constant $N_y/n=32$ showing the scaling behavior.

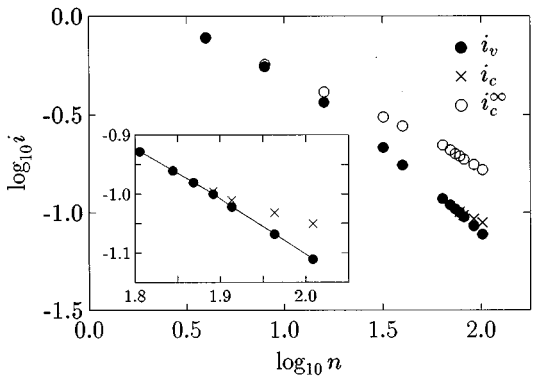

FIG. 5. A plot of critical currents i_v (●) and i_c (×) vs n for a 16×256 array. For $n\simeq74, i_c=i_v$. Also shown are i_c^∞ values (○) using corrections for finite N_x from Fig. 4. The inset shows a magnified region where i_v and i_c bifurcate. The smooth line through (●) symbols is a guide to the eye.

64 to 128 for $n=8$ and $n=2$, respectively. From Fig. 4, we see that i_c scales in N_x/n and that, furthermore, for $n\simeq 2N_x$, $\Delta i_c/i_c^\infty$ is $\gtrsim 30\%$. This can be understood as follows. The current injected at the left edge of the array must flow around the defect. The smaller the value of N_x, for a given defect size, the larger the curvature of the current flow lines around the defect and hence the larger the vorticity $\partial i_x/\partial y$. Since i_c is related to nucleation of vortices, and this occurs more easily for an enhanced vorticity, i_c diminishes, if N_x is reduced keeping n fixed.

A similar reduction in i_c also occurs with decreasing N_y for a given N_x/n because current redistribution away from the defect gets increasingly constrained. In Fig. 4, the error in i_c due to the finiteness of N_y is $\sim 0.01\%$.

The effects of a sharp increase in vorticity near the tip of the defect are dramatically exhibited by the formation and flow of vortices *along* rather than perpendicular to the direction of $i_{\rm ext}$. This is observed for small values of N_x/n for which the current flowing near the tip has a large $\partial i_x/\partial y$ component. This in turn produces large values of both i_y and $\partial i_y/\partial x$. As a result, pairs of vortices [both of the same sign due to the symmetry $\theta(-x,y)=-\theta(x,y)$ about the y axis] nucleate at the sides of the tip for $i>i_c$, and flow in opposite directions along the x axis. This phenomenon can be observed, for example, in an 8×128 array with $n=48$ and $i_{\rm ext}=0.15$.

Having shown that in long narrow arrays with moderate-sized defects, i_p increases and surpasses i_v, while i_c in general decreases, we turn to a detailed study of the vortex-pinning regime $(i_c>i_p>i_{\rm ext}>i_v)$. For concreteness, we specialize all our observations to a 16×256 array with 100 missing bonds. We find that the vortex which appears at the tip of the defect for $i_{\rm ext}=i_v$ is always unstable there and moves up the corridor as soon as it forms. However, it gets pinned 15 plaquettes away from the defect and all voltages then quickly drop to zero. The phases along the LECC are now configured as follows: Those preceding the vortex are all in the second and third quadrants while those following it are in a decreasing sequence lying entirely in the first quadrant [similar to the configuration shown in Fig. 3(b), except that the vortex is now outside the defect]. A continuous enhancement in $i_{\rm ext}$ sees each of these angles increasing continuously. Whenever the phase difference across the upper edge of the plaquette containing the vortex becomes π, the current through it changes from being parallel to $i_{\rm ext}$ to being antiparallel and the vortex moves up by one plaquette. Likewise, when $2\theta_{\rm tip}$ reaches the value $(2k+1)\pi, k=1,2,\ldots,$ the kth vortex is nucleated at the tip of the defect. This vortex immediately moves up the corridor pushing the other vortices ahead of itself upward. All the vortices which are thus set into motion eventually get pinned and the transient time dependence in voltage disappears. The process continues until (for the above-mentioned values of N_x, N_y, and n) a maximum of five vortices are pinned by the lattice. Thereafter, for $i_{\rm ext}>i_c$, the vortex street begins to run with a definite periodicity. It is noteworthy that in the periodic domain, the minimum number of vortices simultaneously present in the central corridor either equals or exceeds by one the maximum number pinned in the steady-state regime.

The vortex train formed in the CC is found to be unstable in long narrow arrays at any finite temperature (the rounding off errors in numerical simulations are equivalent to a small but finite temperature). For long narrow arrays (e.g., 4×32), the vortices in the CC are close together, typically 3–4 lattice spacings apart. This is because the image charges across the edges in the narrow dimension screen the vortex charges in the CC. As the position of a given vortex inside its plaquette fluctuates away from the center, $x=0$, it experiences a destabilizing force, due to y-bond currents in this plaquette, produced by the other vortices in the CC. This current is large enough (owing to the proximity of these vortices) to overcome the pinning force in the x direction. The images of the vortex across the width of the array are also sufficiently close to exert a force which further helps the destabilization process. The linear chain of the vortices in the CC is thus rendered unstable. This instability is also seen in wider arrays with long linear defects, which create appreciable y-bond currents in the plaquettes along the CC close to the tip of the defect.

Finally in this section, we consider the asymptotic dependence of i_c on the defect size n, particularly in the presence of pinned vortices. Since vortices redistribute the current, increasing its value away from the defect, they could conceivably make the defect effectively larger.[16] On the contrary we find that, as far as i_c is concerned, the effective size of the defect is *reduced* by pinned vortices. We plot i_c versus n in Fig. 5 for a 16×256 array. For $n\lesssim74$, the vortices cannot be

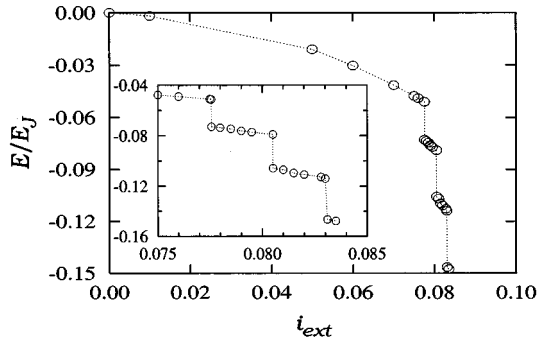

FIG. 6. The energy per bond in a 16×256 array with an $n=100$ defect as a function of $i_{\rm ext}<i_c$. Discontinuities appear at each transition from one vortex sector to the next. The inset shows a magnified transition region.

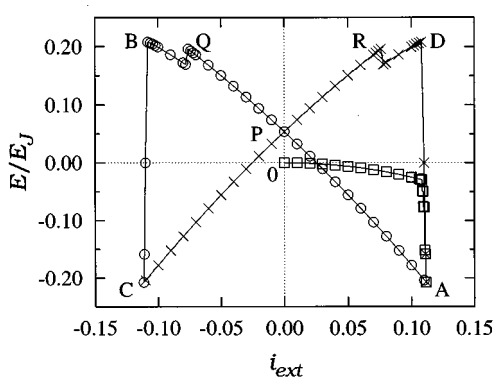

FIG. 7. The energy per bond of a 8×256 array with an $n=50$ defect as a function of $i_{\rm ext}<i_c$ showing hysterisis. The various ranges of $i_{\rm ext}$ traversed in the given order are (□) $0\rightarrow i_{\rm max}$, (○) $i_{\rm max}\rightarrow -i_{\rm max}$, (×) $-i_{\rm max}\rightarrow i_{\rm max}$.

pinned as $i_c(=i_v)$ is larger than i_p, while for $n\gtrsim74$, they can. Hence, for $n>74$, we plot both i_v (full circles) and i_c (crosses). It is seen that while the values of i_v follow the curve smoothly across the value $n=74$, those of i_c bifurcate from and lie above this curve. This increase in i_c relative to i_v shows that the effective size of the defect is reduced by the pinned vortices. The extrapolated values of i_c^∞ using the results of Fig. 4 are also shown. Each of these values is larger than $i_p^\infty(\simeq0.1)$. It follows that defects of size much larger than 74 would be needed to observe pinning in infinite arrays: The estimate of Leath and Xia[16] is in the right ballpark.

C. Energy of the system and hysteresis

The energies of the static configurations forming the steady-state regime of a bond-diluted array acquire, in the presence of pinned vortices, a range of interesting features which we now investigate. As mentioned in Sec. III B, a vortex which forms at $i_{\rm ext}=i_v$ never stabilizes at the point of nucleation (the tip of the defect for the case of broken bonds) and moves a certain distance along the CC before getting pinning. Thus the variation of the phases in the CC (and elsewhere) is discontinuous between i_v^- and i_v^+. It follows that the energy per bond of the system defined as[33]

$$\frac{E}{E_J}=\frac{1}{N_b}\sum_{\langle i,j\rangle}[1-\cos\theta_{ij}]-\frac{i_{\rm ext}}{N_b}\sum_{i,\ j=(N_x+1)/2}[\theta_{i,-j}-\theta_{i,j}] \tag{5}$$

registers a downward discontinuity at the formation and eventual pinning of each new vortex. Here, N_b is total number of bonds in the array. The energy versus $i_{\rm ext}$ graph (see Fig. 6 for a 16×256 array with an $n=100$ defect) can thus be conveniently divided into different sectors with the pth sector having p pinned vortices. The energy decreases continously within a given vortex sector and registers a kink discontinuity only where one enters a higher vortex sector. Moreover, the difference between successive values of $i_{\rm ext}$, at which these kinks occur, decreases continuously, while the energy discontinuity itself becomes larger and larger.

These observations suggest that for an infinite array (or one which is infinite in the y direction, at least), there would be an infinite number of vortex sectors. The total energy of the system for any of these sectors would be infinite, but the energy *differences* would be finite and well defined. However, the sequence E_p of energy-gap values would diverge for $p\rightarrow\infty$. On the other hand, the sequence of $i_{\rm ext}$ values marking transitions from one vortex sector to another would rapidly converge to the depinning current, i_p^∞, for a single vortex in a perfect array. The spacing between vortices pinned by the lattice would increase with distance from the defect and would become infinite for those furthest out. The vortex-vortex interaction, which inevitably comes into play for finite separation between vortices, would thus become negligible at large distances from the defect.[34] It is because of this that the infinite vortex street would be set into motion only by i_p^∞.

Finally, once vortices have formed and stabilized at various pinning sites in the presence of a certain $i_{\rm ext}$, they will remain as configured even when this current is reduced to zero. There are consequently at least two configurations of the array at $i_{\rm ext}=0$ with different values of energy. The actual number is, of course, much larger. In fact there are as many states as there are allowed vortex configurations in the time-independent regime of the given array. The energy is, therefore, multiple valued in $i_{\rm ext}$ and the $i_{\rm ext}$–E curve is, in this sense, hysteretic. A typical graph, for an array of size 8×256 with 50 broken bonds, is shown in Fig. 7. We note that this graph is symmetric about the E axis. In plotting it, we first raise $i_{\rm ext}$ from 0 to $i_{\rm max}$, a current for which there are 5 pinned vortices in the array, and obtain section OA of the hysteresis curve. We next decrement the current from $i_{\rm max}$ through 0 to $-i_{\rm max}$ (curve $APQBC$) and finally raise it back to $i_{\rm max}$ (curve $CPRDA$). The hysteresis loop so obtained is found to be independent of the size of the current step used in tracing it.

The various features of the closed curve displayed in Fig. 7 are understood as follows. A set of 5 vortices forms and stabilizes over part OA, as described above. There is no change in the positions of these vortices as the array goes from A to Q. However, the system's energy increases steeply (so much so that at $i_{\rm ext}=0$, corresponding to point P in Fig. 7, the energy is positive). Both circumstances persist until we come close to Q, wherein one of the vortices gets annihilated by the antivortex nucleated at the tip of the defect decreasing its energy. Slightly short of this point, antivortices steadily begin nucleating at the tip of the defect. Once this happens,

the vortices originally present in the CC rapidly disappear through vortex-antivortex annihilation and their positions are taken shortly thereafter by antivortices. The energy of the array suffers a sharp drop in the process. For $i_{ext}=-i_{max}$, this energy is negative and equal to its value at i_{max}. Since the figure is symmetric about $i_{ext}=0$, a similar process occurs during the branch $CPRDA$ with the vortices now anihilating the antivortices present in the array. Interestingly enough, at our level of resolution in i_{ext}, we do not encounter, at any point of the hysteresis loop, a regime in which there are no vortices present in the array. Finally, it should be pointed out that hysteresis loops of this kind are not uncommon among superconducting systems.[35]

D. The periodic regime

In this section we examine the periodic regime of arrays with linear defects and study the mechanism of propagation of vortices in the CC. Once the system enters the time-dependent state (for $i_{ext}>i_c$), vortices nucleate and peel off periodically from the tip of the defect, traverse the entire length of the corridor and pass out of the array.[16] All the phases in the array rotate at the same average angular velocity, ω, where the averaging is done over a time period. The angular velocity is *not constant* since that would imply that the supercurrent in each link is independent of time.

A snapshot of the phases in an array of size 32×128 with an $n=8$ defect is shown in Fig. 8. All the phases to the left of the CC rotate anticlockwise while those on the right rotate clockwise. The phases along the columns of the array form ''spin waves'' moving in the positive y direction, while the phases along the rows constitute spin waves converging onto the CC. The resultant spin waves, therefore, seemingly form a wake, but actually move into the vortex and propel it forward. In Fig. 8, the wave fronts corresponding to the spin waves can be seen easily as dark streaks running across the picture. However, these wave fronts are *ahead* of the vortex rather than behind it. The situation is akin to a time-reversed motion of a boat moving in water. Whereas the boat provides the energy to propel itself forward while transfering some of it to the waves in the wake, here the vortex absorbs energy to move forward from the spin waves present in the JJA. The ''wake'' here is asymmetric about the y axis as a vortex has the special property of changing the phase by π across the plaquette containing it.

The nature of the waves discussed here is different from those in arrays with capacitive junctions.[36,37] In such arrays, a vortex moving across a plaquette induces voltages on the superconducting islands, which keep oscillating due to stored capacitive energy long after the vortex has moved away. Thus, vortices (having a finite mass in capacitive arrays) can interact with each other through these spin waves. In overdamped arrays, the vortices just ''ride'' the spin waves described in this paper. In capacitive arrays, we observe that the inertial oscillations are superimposed upon the waves that the vortices ride.

The separation between successive vortices along the CC is $\lambda/2$, where λ is the wavelength for spin waves in that direction. The frequency ω is roughly proportional to $1/\lambda$. The value of λ is, however, affected by edges. It increases monotonically as one moves towards the boundary. This is because the frequency of the periodic regime is constant at ω (for a given i_{ext}) while the speed of vortices is higher near the edges due to attraction from the image charges across the latter.

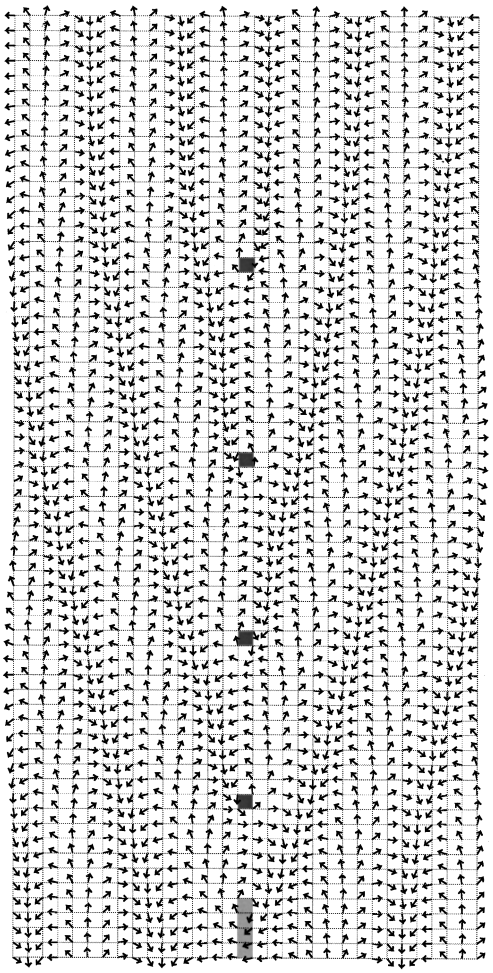

FIG. 8. A snapshot of a 32×128 with $n=8$ array in the periodic regime. The arrows represent the phases at the superconducting sites. The defect is the lightly shaded region. The dark shaded plaquettes are occupied by vortices. The wave fronts corresponding to the spin waves are seen as dark streaks across the picture and form a wake in front of the vortices. Note that the wake is asymmetric about the y axis.

In the x direction, the phases wind with a finite wavelength even in the steady-state regime. This static configuration corresponds to a wavelength which decreases monotonically with an increase in i_{ext}. As i_{ext} crosses i_c, this ''frozen'' spin wave starts moving. Consequently, at $i_{ext}=i_c$, $\omega=0$, but the wavelength in the x direction is finite. Similarly a finite wavelength along the y direction would also exist for $\omega=0$ in the case of sufficiently large arrays where pinned vortices in the CC are present in the steady-state regime (and the transition from steady state to periodicity takes place through an n-vortex sector with finite n, as described in Sec. III C above).

The angle subtended by the wake at each vortex can be deduced from the ratio of the wavelengths in the y and x directions. As expected, this angle decreases as the vortices move faster under an increase in i_{ext}.

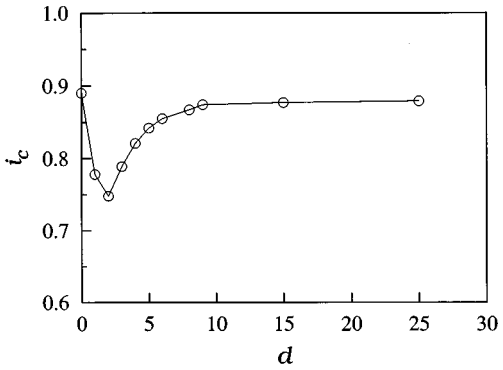

FIG. 9. The critical current i_c vs the separation d between defects. The line through the data points is a guide to the eye.

IV. DISTRIBUTED DEFECTS

We now turn to more complicated defect patterns with a view to determining the dependence of i_c on defect shape and size and distribution. In doing this, we shall find it useful to keep in mind the analogies, brought out by Mehrotra and Shenoy,[38,39] between current flow in JJA's and hydrodynamic flow through a pipe. These authors consider nonuniformly driven JJA's at zero temperature. They find that the linear gradient of the external current drive, $\partial i_x/\partial y$ is a measure of injected vorticity which, multiplied by the y dimension of the array (pipe diameter), and scaled by the inverse shunt resistance gives the analog of the Reynold's number. They further note that the chaotic behavior observed above a certain injected-vorticity threshold is, as in turbulent fluid flows, due to a mixing of positive and negative vortices. In the spirit of this analogy, we now liken current flows past bond diluted-disordered linear defects to fluid flows past obstacles. Such current flows are closely related to those explored in Ref. 39 because the defect automatically creates a nonzero current gradient, $(\partial i_x)/(\partial y)$. We examine effects of streamlining and find that similarities with fluid flow continue to exist.

We study the bond diluted case by grading defective bonds with a $g\rightarrow 0$ (we use $g=10^{-7}$, in actual practice) rather than by eliminating them. This permits the use of faster algorithms and makes no difference to the i_c values we are interested in. Indeed, only supercurrents flow through the bonds in the time independent state, and even these turn off wherever g is set to zero.

To determine the effect on i_c of the distance between defects, we consider the case of two highly graded x bonds ($g=10^{-7}$), placed in the central column with an interdefect separation d (each of the missing bonds is an $n=1$ defect). A plot of i_c versus d (Fig. 9) shows a minimum at $d=2$. As both defects try to force current away from themselves, a ''squeezing'' of current into the channel between the two defects occurs resulting in a ''breakdown'' inside the channel. This is similar to hydrodynamic flow through a narrow passage. For $d\lesssim 2$, the channel is too narrow (compared to the ''viscous penetration depth'') for current to flow through and the two defects are seen as just one large defect. This causes an initial decrease in i_c. For $d\gtrsim 2$, the current starts flowing through the channel. For large values of d, the two defects become independent of each other and i_c approaches its value for a single defect.

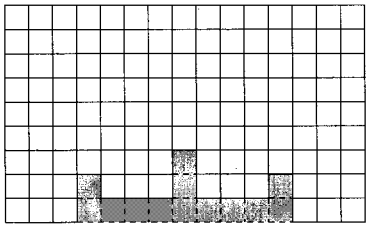

FIG. 10. Schematic of the $y>0$ section of an array with a typical defect $(4,3-2,6,3-2,4)$ used to study streamlining. Each side of dotted squares denotes a Josephson junction. The junctions marked with a cross are graded with $g=10^{-7}$ and are equivalent to broken bonds.

In studying the effects of streamlining, we use the following notation to denote defect configurations. A sequence of numbers $a,m-b,c,m-b,a$ corresponds to a defect placed at the center of the array, with c graded x bonds in the central corridor, m columns of b graded x bonds each followed by a single column of a graded x bonds, on either side of the CC. A typical defect configuration $(4,3-2,6,3-2,4)$ is shown in Fig. 10.

Our results are shown in Fig. 11 where the values of i_c are plotted versus m for two distinct cases. We first consider the $4,m-0,6,m-0,4$ class of defects which corresponds to placing an $n=4$ defect in front of an $n=6$ defect, along the injected current path. For $m=0$, the i_c value is 0.592, which is 0.025 higher than $i_c^{(6)}$ the value for a single $n=6$ defect (shown by the solid line in the figure). As m is increased, i_c goes through a maximum at $m=m_{\max}=2$ and then decreases asymptotically to $i_c^{(6)}$ A second class of defects $4,m-2,6,m-2,4$ shows a similar trend, except that the asmyptotic value now corresponds to the value for the $\infty-2,6,\infty-2$ defect (the dotted line actually represents measurements on a $15-2,6,15-2$ defect). It should be noted that while the second class has more defective bonds than the first, the i_c values of the former are *higher* than those of the latter, for all m.

The above results are consistent with hydrodynamic flows and can be understood as follows. Any reduction in the curvature and y gradient of current density in the x direction, $(\partial i_x/\partial y)$, increases the value of i_c, as it corresponds to an improved streamlining of the current flow. For example, the i_c value for $m=0$ (see Fig. 11) is higher than $i_c^{(6)}$. Similarly, rectangular defects have higher i_c's when aligned along the current direction as opposed to being perpendicular.[40] As m increases to $m_{\max}$, i_c increases further because of even better streamlining. The current flow does not sense the small separation between the $n=4$ and $n=6$ defects and does not enter the interdefect region significantly. For $m>m_{\max}$, the current starts penetrating this region and in going around the $n=6$ defect produces a larger value of $\partial i_x/\partial y$. This in turn decreases the values of i_c. For large values of m, the defects becomes independent and hence i_c asymptotically approaches the dotted line. As the current flow lines cannot bend back into the region between the $n=6$ and $n=4$ defects far enough in the second class of defects, the i_c values are higher than the corresponding ones in the first class, for all m.

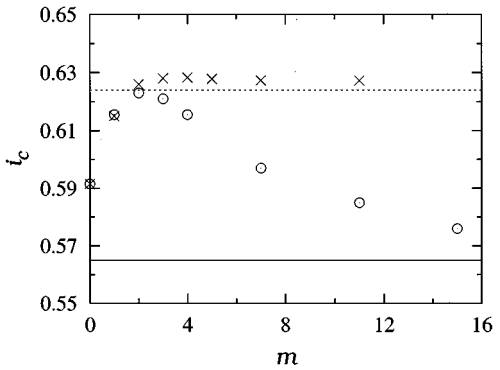

FIG. 11. The variation of i_c with m used to study streamlining. The symbols used relate to ($\bigcirc$) $4,m-0,6,m-0,4$ defects and ($\times$) $4,m-2,6,m-2,4$ defects. The solid line corresponds to $i_c^{(6)}$, the i_c value for a single $n=6$ defect while the dotted one corresponds to the i_c value for a $0,15-2,6,15-2,0$ defect.

V. SUMMARY AND CONCLUSIONS

In conclusion, we have systematically studied JJA's with defects. Using a fast algorithm we have investigated the steady-state regime, the pinning of vortices, the hysteresis present in such arrays and the periodic regime for the case of bond diluted or disordered defects. For bond-disordered arrays with linear defects we have shown that for $g<g_m$ vortex pinning increases its stability against breakdown. In the case of bond-diluted linear defects, we have shown that (i) i_c scales with N_x/n (for fixed N_y/n), (ii) vortices can be pinned in smaller arrays than thought earlier, (iii) for narrow (small N_x/n) arrays the vorticity at the tip of the defect can increase to a point where vortices form and move along the injected current direction, (iv) the presence of pinned vortices increases the supercurrent carrying capacity of the array, (v) the energy of these arrays registers a discontinuous drop at each transition from one vortex sector to a higher one, and (vi) these pinned vortices cause hysteresis. An investigation of the periodic regime of such arrays shows the presence of waves which propel the vortices forward. The studies of distributed defects have shown that an improved streamlining can enhance the magnitude of i_c for the system analogously to hydrodynamic flows.

Several directions for further research are possible. First, a theoretical understanding of the steady-state regime based on a fixed point analysis of the underlying equations is desirable. An in depth investigation of the periodic regime is next. Phenomena like bunching and debunching of several vortices in the column-switched regime as also the occurence of symmetry breaking[26] merit deeper study. These and other related issues are currently under active investigation.

[1] *Proceedings of the NATO Advanced Research Workshop on Coherence in Superconducting Networks*, Delft, The Netherlands, 1987, edited by J. E. Mooij and G. B. J. Schon [Physica B **152**, 1 (1988)]; recent reviews in *Proceedings of the Mini Workshop on Josephson Junction Arrays*, Trieste, Italy, 1995 [Physica B (to be published)].

[2] H. S. J. van der Zant, F. C. Fritschy, T. P. Orlando, and J. E. Mooij, Phys. Rev. Lett. **66**, 2531 (1991).

[3] P. Minnhagen, Rev. Mod. Phys. **59**, 1001 (1987).

[4] K. K. Mon and S. Teitel, Phys. Rev. Lett. **62**, 673 (1989).

[5] S. Teitel and C. Jayaprakash, Phys. Rev. Lett. **51**, 1999 (1983).

[6] W. Xia and P. L. Leath, Phys. Rev. Lett. **63**, 1428 (1991).

[7] D. Dominguez, J. V. José, A. Karma, and C. Weicko, Phys. Rev. Lett. **67**, 2367 (1991).

[8] D. Dominguez, Phys. Rev. Lett. **72**, 3096 (1994).

[9] M. G. Forrestor, H. J. Lee, M. Tinkham, and C. J. Lobb, Phys. Rev. B **37**, 5966 (1988).

[10] B. Berge, H. T. Diep, A. Ghazali, and P. Lallemand, Phys. Rev. B **34**, 3177 (1986).

[11] J. S. Chung, K. H. Lee, and D. Stroud, Phys. Rev. B **40**, 6570 (1989).

[12] Y. H. Li and S. Teitel, Phys. Rev. Lett. **67**, 2894 (1991).

[13] E. Granato and J. M. Kosterlitz, Phys. Rev. B **33**, 6533 (1986).

[14] S. P. Benz, M. G. Forrestor, M. Tinkham, and C. J. Lobb, Phys. Rev. B **38**, 2869 (1988).

[15] D. C. Harris, S. T. Herbert, D. C. Stroud, and J. C. Garland, Phys. Rev. Lett. **67**, 3606 (1991); Physica B **165 & 166**, 1643 (1990).

[16] P. L. Leath and W. Xia, Phys. Rev. B **44**, 9619 (1991).

[17] P. M. Duxbury, P. L. Leath, and P. D. Beale, Phys. Rev. B **36**, 367 (1987).

[18] Sujay Datta, Shantilal Das, Deshdeep Sahdev, and Ravi Mehrotra, Mod. Phys. Lett. **10**, 451 (1996).

[19] W. C. Stewart, Appl. Phys. Lett. **12**, 277 (1968).

[20] D. E. McCumber, J. Appl. Phys. **39**, 3113 (1968).

[21] S. R. Shenoy, J. Phys. C **18**, 5163 (1985); **20**, 2479(E) (1987).

[22] H. Eikmans and J. E. van Himbergen, Phys. Rev. B **41**, 8927 (1990).

[23] Sujay Datta, Shantilal Das, Deshdeep Sahdev, Ravi Mehrotra, and Subodh Shenoy, Phys. Rev. B **54**, 3545 (1996).

[24] W. H. Press, S. A. Teukolksy, W. T. Vetterling, and B. P. Plannery, *Numerical Recipes* (Cambridge University Press, Cambridge, 1986).

[25] The calculations were done on a Hewlett Packard 9000 series model 735 workstation.

[26] The symmetry $\theta(x,y)=\theta(-x,y)$ also exists and could be exploited. However, we have found that if the array is driven into the chaotic region, the symmetries about the x and y axes are broken. We monitor both $\theta(x,y)$ and $\theta(-x,y)$ to ascertain that the array is not driven chaotic. Details of this phenomenon will be published elsewhere.

[27] D. Dominguez and J. V. José, Int. J. Mod. Phys. B **8**, 3749 (1994).

[28] D. Dominguez and J. V. José, Phys. Rev. B **48**, 13 717 (1993).

[29] V. Ambegaokar and A. Baratoff, Phys. Rev. Lett. **10**, 486 (1963); **11**, 104(E) (1963).

[30] R. C. Budhani, M. Shenaga, and S. H. Liou, Phys. Rev. Lett. **69**, 3816 (1992); R. C. Budhani, S. H. Liou, and Z. X. Cai, *ibid.* **71**, 621 (1993).

[31] C. J. Lobb, David W. Abraham, and M. Tinkham, Phys. Rev. B **27**, 150 (1983).

[32] M. S. Rzchowski, S. P. Benz, M. Tinkham, and C. J. Lobb, Phys. Rev. B **42**, 2041 (1990).

[33] V. Ambegaokar and B. I. Halperin, Phys. Rev. Lett. **22**, 1364 (1969); **23**, 274(E) (1969).
[34] Ravi Mehrotra, Sujay Datta, and Deshdeep Sahdev (unpublished).
[35] I. Dhingra, V. N. Moorthy, and B. K. Das, Supercond. Sci. Technol. **8**, 252 (1995).
[36] U. Eckern and A. Schmid, Phys. Rev. B **39**, 6441 (1989).
[37] U. Eckern and E. B. Sonin, Phys. Rev. B **47**, 505 (1993).
[38] R. Mehrotra and S. R. Shenoy, Europhys. Lett. **9**, 11 (1989).
[39] Ravi Mehrotra and Subodh R. Shenoy, Phys. Rev. B **46**, 1088 (1992).
[40] M. B. Cohn, M. S. Rzchowski, S. P. Benz, and C. J. Lobb, Phys. Rev. B **43**, 12 823 (1991).